

Coherent FDA Receiver and Joint Range-Space-Time Processing

Wenkai Jia, Andreas Jakobsson, *Senior Member, IEEE*, Wen-Qin Wang, *Senior Member, IEEE*

Abstract—When a target is masked by mainlobe clutter with the same Doppler frequency, it is difficult for conventional airborne radars to determine whether a target is present in a given observation using regular space-time adaptive processing techniques. Different from phased-array and multiple-input multiple-output (MIMO) arrays, frequency diverse arrays (FDAs) employ frequency offsets across the array elements, delivering additional range-controllable degrees of freedom, potentially enabling suppression for this kind of clutter. However, the reception of coherent FDA systems employing small frequency offsets and achieving high transmit gain can be further improved. To this end, this work proposes an coherent airborne FDA radar receiver that explores the orthogonality of echo signals in the Doppler domain, allowing a joint space-time processing module to be deployed to separate the aliased returns. The resulting range-space-time adaptive processing allows for a preferable detection performance for coherent airborne FDA radars as compared to current alternative techniques.

Index Terms—Frequency diverse array (FDA), Doppler orthogonality, airborne radar, space-time adaptive processing.

I. INTRODUCTION

MOVING target indication (MTI) techniques are used for ground-based radar to separate moving targets and stationary ground clutter by performing band-stop filtering in the time domain or in the Doppler domain. Weighting each element, spatial filtering enables the array antenna to enhance the desired signal while rejecting unwanted interfering signals from a given direction of arrival (DOA). However, the ground clutter seen by an airborne radar spreads within the Doppler region due to the platform motion, making it more difficult to decide whether a target is present in a given observation as potential targets may be masked by mainlobe clutter with the same angle as the target and by sidelobe clutter from the same Doppler frequency [1]. One may employ space-time adaptive processing (STAP) using spatial and temporal degrees of freedoms in order to adjust the two-dimensional space-time receiving filter weights in an attempt at maximizing the filter's output SINR, thereby improving the radar detection capacity [2]. Regrettably, when the target is in the mainlobe of the antenna, although the clutter spectrum is basically a narrow ridge, slow targets will fall into the resulting stop-band, thereby causing performance degradation.

This work was supported in part by National Natural Science Foundation of China 62171092.

Wenkai Jia and Wen-Qin Wang are School of Information and Communication Engineering, University of Electronic Science and Technology of China, Chengdu, 611731, P. R. China. (e-mail: wenkai.jia@matstat.lu.se; wqwang@uestc.edu.cn).

Andreas Jakobsson is with the Division of Mathematical Statistics, Center for Mathematical Sciences, Lund University, SE-22100 Lund, Sweden. (e-mail: andreas.jakobsson@matstat.lu.se).

The use of frequency diverse arrays (FDAs), first proposed by Antonic *et al.* [3], [4], using small frequency offsets (FOs) across the elements, has proven to be advantageous in mainlobe interference suppression [5], [6], joint estimation of range and angle [7]–[9], and target tracking [10], [11]. This gain result from the possibility to also exploit the available and controllable degrees of freedom in the range dimension. From a transmission perspective, the key aspect of FDA is that a range (or delay) increment along a certain direction translates into a relative phase progression among identical sources, making it possible to achieve a focused beampattern in the desired range-angle plane by designing the FOs appropriately [12]–[15]. However, the processing of the FDA echoes is involved due to the need to separate the resulting aliased multi-carrier signals. This difficulty may be avoided in the case when the FO is larger than the bandwidth of the baseband waveform [16]–[18]. Since the spectra do not overlap in this case, a low-pass filter is then able to separate the components without difficulty, although this gain comes at the price of an increased bandwidth. For a co-located MIMO, which transmits mutually orthogonal waveforms, the reception procedure used by an FDA-MIMO cause a loss in the resulting transmission gain. Various approaches have been introduced to handle the received signals, such as the multichannel matched filtering structure presented in [19], where each receive antenna is implemented by a group of carriers with matched filters. These may be applied to FDA systems using arbitrary FOs, including linear or nonlinear ones. However, for small FO, the necessary requirement of waveform orthogonality for all Doppler and delay pairs makes such a solution infeasible in practice.

In this paper, we focus on the application of range-space-time processing for airborne coherent FDA radars, introducing a receiver that exploits the orthogonality in the Doppler domain. As even small FOs will destroy orthogonality and the coherence of the waveforms, the fast-time receiving structure will not be able to deal with the aliased returns. Different from the multi-channel filtering or the low-pass filtering receiver, where the returns are only processed in the fast-time, the here proposed receiver jointly filters the returns in the space-time domain. We initially consider a pulsed-FDA transmit signal with a coded phase for each element, although it is worth noting that the here introduced phase code is different from the space-time coding technique in [20], which aims at shifting the frequency band of each pulse to synthesize a full bandwidth, thereby improving the range resolution. The here proposed phase encoding scheme instead imparts an additional Doppler shift to the pulsed signal transmitted by each antenna. Then, in the receiver, after processing the

received signal using multi-carrier mixing and applying the matched filtering in the fast-time domain, the subsequent steps include the Doppler demodulation and a low-pass filtering in the slow-time, i.e., the inter-pulse time domain. The resulting joint space-time processing is capable of separating the aliased returns without any additional constraints on the FO or on the transmit waveforms, yielding a coherent FDA range-space-time signal model. Numerical simulations demonstrate the effectiveness of proposed receiver for coherent FDA and an achievable high-gain detection of slow moving targets that would be obscured by the clutter ridge of a conventional airborne STAP radar.

The remainder of the paper is organized as follows. In Section II, we briefly review conventional receiving schemes and their suitability for FDA-MIMO and for coherent FDA array systems. In Section III, we introduce the proposed FDA receiver based on joint space-time processing to efficiently receive FDA returns. In Section IV, considering an airborne FDA radar, the resulting interference and noise models are analyzed, and a weight-based FDA range-space-time processing scheme is developed. Simulation results are given in Section V. Finally, in Section VI, we present our conclusions.

II. BACKGROUND

Consider a uniformly spaced linear FDA radar with N_T transmit antennas measuring the backscattering resulting from transmitters using an uniform FO with central carrier frequency f_c , each of which emits the same narrowband waveform, $u(t)$, having unit energy, i.e., $\int_{T_p} |u(t)|^2 dt = 1$, where T_p denotes the pulse duration. The transmitted signal, $s(t)$, may then be expressed as

$$s(t) = \sum_{m=1}^{N_T} w_m u(t) e^{j2\pi(f_c + (m-1)\Delta f)t} \quad (1)$$

where w_m and Δf denote the transmit weight of the m -th antenna and the FO, respectively. Assuming a far-field point target located at the angle-range pair (θ_t, r_t) , the reflected signal, $\bar{s}(t)$, may be expressed as

$$\begin{aligned} \bar{s}(t) &= s\left(t - \left(\frac{r_t}{c} - (m-1)\frac{d_t \sin \theta}{c}\right)\right) \\ &= \sum_{m=1}^{N_T} \left\{ w_m u\left(t - \left(\frac{r_t}{c} - (m-1)\frac{d_t \sin \theta}{c}\right)\right) \right. \\ &\quad \times \left. e^{j2\pi(f_c + (m-1)\Delta f)\left(t - \frac{r_t}{c} + (m-1)\frac{d_t \sin \theta}{c}\right)} \right\} \\ &\approx e^{j2\pi f_c\left(t - \frac{r_t}{c}\right)} u\left(t - \frac{r_t}{c}\right) \\ &\quad \times \sum_{m=1}^{N_T} w_m e^{j2\pi(m-1)\Delta f\left(t - \frac{r_t}{c}\right)} e^{j2\pi(m-1)(f_c + \Delta f)\frac{d_t \sin \theta}{c}} \end{aligned} \quad (2)$$

where d_t denotes the spacing between the transmit antennas. For an FDA receiver with N_R equally spaced receive antennas, the resulting backscattered signal arriving at its n -th antenna

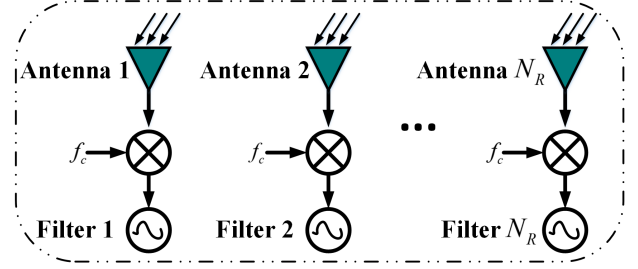


Fig. 1. The receiver for FDA-MIMO system.

may then be approximated as

$$\begin{aligned} y_n(t) &= \delta_t \bar{s}\left(t - \left(\frac{r_t}{c} - (n-1)\frac{d_r \sin \theta}{c}\right)\right) \\ &\approx \delta_t e^{j2\pi f_c\left(t - \frac{2r_t}{c}\right)} e^{j2\pi(n-1)f_c\frac{d_r \sin \theta}{c}} u\left(t - \frac{2r_t}{c}\right) \\ &\quad \times \sum_{m=1}^{N_T} w_m e^{j2\pi(m-1)\Delta f\left(t - \frac{2r_t}{c}\right)} e^{j2\pi(m-1)(f_c + \Delta f)\frac{d_t \sin \theta}{c}} \end{aligned} \quad (3)$$

where δ_t and d_r denote the target's complex-valued reflection coefficient and the spacing between the receive antennas, respectively. It should be noted that δ_t may be decorrelated in frequency as a result of the FDA's multi-carrier transmission mechanism, although a sufficient condition to avoid the frequency decorrelation for an FDA radar with linear FO is [21]

$$\Delta f \leq \frac{c}{4(N_T - 1)\Delta \varsigma} \quad (4)$$

where $\Delta \varsigma$ denotes the target length along the radar's boresight.

Fig. 1 shows an FDA-MIMO system, i.e., a receiver structure fully utilizing the orthogonality of the signal in the frequency domain in the case the FO is larger than the base-band bandwidth. For each receive antenna, the returned FDA signals are demodulated using the central carrier frequency, f_c , followed by a suitable band-pass filter. As a result, the output of the n -th receive antenna can be expressed as

$$\begin{aligned} \bar{y}_n(t) &= (y_n(t) \cdot e^{-j2\pi f_c t}) * h_n^c(t) \\ &= \delta_t e^{-j2\pi f_c \frac{2r_t}{c}} e^{j2\pi(n-1)f_c \frac{d_r \sin \theta}{c}} \\ &\quad \times \left[\kappa_n(t) * h_n^c(t) + \underbrace{\left(\sum_{\substack{m=1 \\ m \neq n}}^{N_T} \kappa_m(t) \right)}_{\text{aliased term}} * h_n^c(t) \right] \\ &= \delta_t e^{-j2\pi f_c \frac{2r_t}{c}} e^{j2\pi(n-1)f_c \frac{d_r \sin \theta}{c}} \kappa_n(t) \end{aligned} \quad (5)$$

where

$$\begin{aligned} \kappa_n(t) &= w_n e^{j2\pi(n-1)(f_c + \Delta f)\frac{d_t \sin \theta}{c}} \\ &\quad \times u\left(t - \frac{2r_t}{c}\right) e^{j2\pi(n-1)\Delta f\left(t - \frac{2r_t}{c}\right)}, \end{aligned} \quad (6)$$

with $*$ and $(\cdot)^c$ denoting the convolution and the conjugate operators, respectively, and where $h_n(t)$ is the used band-pass filter, having passband $f_{pass} \in [(n-1)\Delta f, n\Delta f]$. Since the

FO is larger than the baseband bandwidth, the occupied spectra of the aliased term do not overlap with that of $\kappa_n(t) * h_n^c(t)$ in (5), implying that the filter is capable of extracting the desired signal from the aliased ones. It is worth noting that the receiver uses the same number of receive antennas as transmit antennas, indicating that the virtual array may not be formed.

For the case where the FO is smaller than the baseband bandwidth, [19] proposed a multi-carrier mixing and matched filtering receiver structure. First, the echo signal to the n -th receive antenna, $y_n(t)$, is demodulated by multi-channel mixers with local carrier frequencies $\{f_c + (m-1)\Delta f\}_{m=1}^{N_T}$, which is then matched filtered with the baseband waveform, $u(t)$, to obtain the pulse compression gain. The filter output of m' -th channel of the n -th receive antenna may as a result be expressed as

$$\begin{aligned} \tilde{y}_{n,m'}(t) &= \left(y_n(t) \cdot e^{-j2\pi(f_c + (m'-1)\Delta f)t} \right) * u^c(-t) \\ &= \delta_t o_{n,m'} \int_{T_p} u\left(\tau - \frac{2r_t}{c}\right) u^c(\tau - t) d\tau + \delta_t \\ &\times \underbrace{\sum_{\substack{m=1 \\ m \neq m'}}^{N_T} o_{n,m} \int_{T_p} e^{j2\pi(m-m')\Delta f\tau} u\left(\tau - \frac{2r_t}{c}\right) u^c(\tau - t) d\tau}_{\text{aliased term}} \end{aligned} \quad (7)$$

where

$$\begin{aligned} o_{n,m'} &= w_{m'} e^{-j2\pi f_c \frac{2r_t}{c}} e^{j2\pi(n-1)f_c \frac{d_r \sin \theta}{c}} \\ &\times e^{j2\pi(m'-1)((f_c + \Delta f) \frac{d_t \sin \theta}{c} - \Delta f \frac{2r_t}{c})} \end{aligned} \quad (8)$$

It is worth noting that if

$$\int_{T_p} e^{j2\pi(m-m')\Delta f\tau} u\left(\tau - \frac{2r_t}{c}\right) u^c(\tau - t) d\tau = 0, \quad (9)$$

$\forall t, m \neq m'$

the aliased term in (7) will be filtered, yielding the desired output

$$\tilde{y}_{n,m'}(t) = \delta_t o_{n,m'} \int_{T_p} u\left(\tau - \frac{2r_t}{c}\right) u^c(\tau - t) d\tau \quad (10)$$

However, it may be seen that the orthogonality condition in (9) is so strict that it is impossible to find a suitable waveform $u(t)$ and FO Δf , although it is noted in [19] that for extremely small FOs, the condition can be approximately satisfied, but then with an unavoidable performance loss.

III. PROPOSED RECEIVER FOR COHERENT FDA

The assumed system is a pulsed-Doppler FDA radar on an airborne platform moving with constant velocity v_a , as illustrated in Fig. 2. The N_T transmit antennas and the N_R receive antennas are uniformly arranged along the movement direction of the platform, forming a side-looking airborne FDA radar. In the figure, ψ denotes the conic angle, which satisfies

$$\cos(\psi) = \cos(\theta) \cos(\phi) \quad (11)$$

with θ and ϕ representing the azimuth angle and the depression angle, respectively.

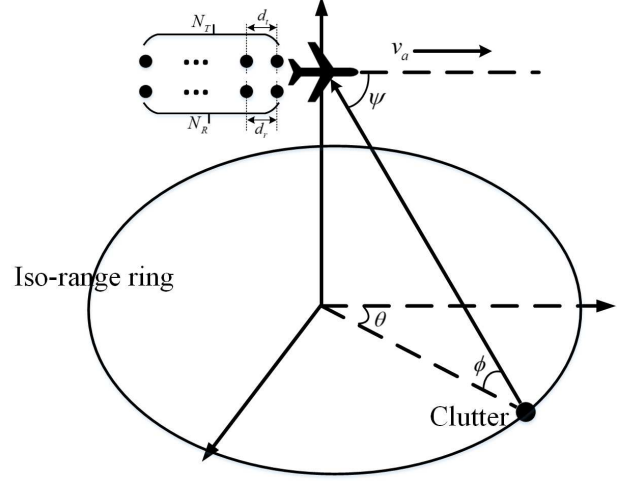


Fig. 2. Geometric model of airborne FDA radar antenna.

A. Transmit Signal Model

The proposed receiver is based on the orthogonality of the received signal in the Doppler domain in order to facilitate the channel separation during pulse compression. Firstly, for each transmit antenna, we introduce the designed phase codes φ_m , for $m = 1, 2, \dots, N_T$. Thus, the l -th pulse transmitted by the N_T antennas can be expressed as

$$s(t_l, \tau) = \sum_{m=1}^{N_T} w_m \text{rect}\left(\frac{\tau}{T_p}\right) u(t) e^{j2\pi((f_c + (m-1)\Delta f)t + \varphi_m t_l)} \quad (12)$$

for $l = 1, 2, \dots, L$, with L denoting the number of pulses, where

$$\text{rect}\left(\frac{\tau}{T_p}\right) = \begin{cases} 1 & |\tau| \leq \frac{T_p}{2} \\ 0 & |\tau| > \frac{T_p}{2} \end{cases}, \quad (13)$$

and with $\tau = t - t_l$ and $t_l = lT_r$ denoting the fast and slow time, respectively, with T_r being the pulse repetition interval (PRI). It is worth noting that the resulting FDA signal is composed of N_T signals with different carrier frequencies $\{f_c + (m-1)\Delta f\}_{m=1}^{N_T}$, each signal consisting of L pulses with induced Doppler φ_m .

B. Echo Signal Model

The target is defined as a point scatterer moving with velocity v_t located at the range-angle pair (r_t, θ_t, ϕ_t) . The target delay $\xi_{m,n,l}$ consists of four components, such that

$$\begin{aligned} \xi_{m,n,l} &= \xi(r_t) + (m-1)\xi_T(\psi_t) \\ &+ (n-1)\xi_R(\psi_t) + \xi_D(\tau) + \xi_D(t_l) \end{aligned} \quad (14)$$

where

$$\xi(r_t) = \frac{2r_t}{c} \quad (15)$$

denotes the round trip delay,

$$\xi_T(\psi_t) = -\frac{d_t \cos(\theta_t) \cos(\phi_t)}{c} = -\frac{d_t \cos \psi_t}{c} \quad (16a)$$

$$\xi_R(\psi_t) = -\frac{d_r \cos(\theta_t) \cos(\phi_t)}{c} = -\frac{d_r \cos \psi_t}{c} \quad (16b)$$

represent the relative delay between the transmit antennas and the relative delay between the receive antennas, respectively, and

$$\xi_D(\tau) = \frac{2v_t\tau}{c} \times f_c \times \frac{1}{f_c} = \frac{f_{t,d}}{f_c}\tau \quad (17a)$$

$$\xi_D(t_l) = \frac{f_{t,d}}{f_c}t_l \quad (17b)$$

are the delays of the target within and between pulses, respectively, where $f_{t,d} = \frac{2v_t}{\lambda}$ denotes the target Doppler with $\lambda = \frac{c}{f_c}$ being the wavelength.

In order to obtain the analytical echo signal model, three assumptions are made, namely

- 1) The radar cross-section (RCS) of the targets within the same coherent processing interval (CPI) do not fluctuate significantly, i.e., the target obeys a Swerling III model [22].
- 2) The envelope delays due to the antenna spacing and the target motion are negligible¹.
- 3) The pulse duration is small enough so that the intrapulse Doppler shift is negligible.

As a result, the l -th pulse transmitted by the m -th transmit antenna reflected to the n -th receive antenna has the form

$$\begin{aligned} y_{m,n}(t_l, \tau) &= \delta_t w_m \text{rect}\left(\frac{\tau - \xi_{m,n,l}}{T_p}\right) u(t - \xi_{m,n,l}) \\ &\quad \times e^{j2\pi((f_c + (m-1)\Delta f)(t - \xi_{m,n,l}) + \varphi_m t_l)} \\ &\approx \delta_t a_{m,n}(\psi_t) w_m \text{rect}\left(\frac{\tau - \xi(r)}{T_p}\right) u(t - \xi(r)) \\ &\quad \times e_m(t - \xi(r)) \omega_{D,m}(t_l, \varphi_m) \end{aligned} \quad (18)$$

where

$$a_{m,n}(\psi_t) = e^{j2\pi(f_c + (m-1)\Delta f)[(m-1)\xi_T(\psi_t) + (n-1)\xi_R(\psi_t)]} \quad (19a)$$

$$e_m(t) = e^{j2\pi(f_c + (m-1)\Delta f)t} \quad (19b)$$

$$\begin{aligned} \omega_{D,m}(t_l, \varphi_m) &= e^{j2\pi[(f_c + (m-1)\Delta f)\xi_D(t_l) + \varphi_m t_l]} \\ &= e^{j2\pi\left(\frac{(f_c + (m-1)\Delta f)}{f_c} f_{t,d} + \varphi_m\right)t_l}. \end{aligned} \quad (19c)$$

This implies that the sum of all N_T signals reflected to the n -th receive antenna may be expressed as

$$\begin{aligned} y_n(t_l, \tau) &= \sum_{m=1}^{N_T} y_{m,n}(t_l, \tau) \\ &= \delta_t \mathbf{a}_n^T(\psi_t) \mathbf{\Omega}(t_l, \varphi) \mathbf{U}(\tau, \xi(r_t); \mathbf{w}) \mathbf{e}(t - \xi(r_t)) \end{aligned} \quad (20)$$

where

$$\mathbf{\Omega}(t_l, \varphi) = \text{diag}\{\omega_D(t_l, \varphi)\} \quad (21a)$$

$$\begin{aligned} \omega_D(t_l, \varphi) &= \\ [\omega_{D,1}(t_l, \varphi_1), \omega_{D,2}(t_l, \varphi_2), \dots, \omega_{D,N_T}(t_l, \varphi_{N_T})]^T, \end{aligned} \quad (21b)$$

with $\text{diag}\{\omega_D(t_l, \varphi)\}$ denoting the diagonal matrix with

entries formed by $\omega_D(t_l, \varphi)$, and where

$$\mathbf{a}_n(\psi_t) = [a_{1,n}(\psi_t), a_{2,n}(\psi_t), \dots, a_{N_T,n}(\psi_t)]^T \quad (22a)$$

$$\begin{aligned} \mathbf{e}(t - \xi(r_t)) &= \\ [e_1(t - \xi(r_t)), e_2(t - \xi(r_t)), \dots, e_{N_T}(t - \xi(r_t))]^T, \end{aligned} \quad (22b)$$

$$\mathbf{U}(\tau, \xi(r_t); \mathbf{w}) = \text{rect}\left(\frac{\tau - \xi(r_t)}{T_p}\right) u(t - \xi(r_t)) \text{diag}\{\mathbf{w}\} \quad (23)$$

with

$$\mathbf{w} = [w_1, w_2, \dots, w_{N_T}]^T \quad (24)$$

denoting the transmit weight vector.

C. Multi-carrier Mixing

To separate the desired signal from the aliased ones, the proposed receiver initially forms a multi-carrier mixing in the fast-time domain. Similar to the receiver in [19], the used mixing frequencies are $\{f_c + (m-1)\Delta f\}_{m=1}^{N_T}$. Thus, the mixed output of the m' -th channel may be expressed as

$$\begin{aligned} r_{m',n}(t_l, \hat{\tau}) &= y_n(t_l, \tau) e^{-j2\pi(f_c + (m'-1)\Delta f)\tau} \\ &= \delta_t \mathbf{a}_n^T(\xi(r_t), \psi_t) \mathbf{\Omega}^{m'}(t_l, \varphi) \mathbf{u}^{m'}(\tau, \xi(r_t); \mathbf{w}) \end{aligned} \quad (25)$$

for $m' = 1, 2, \dots, N_T$, where

$$\mathbf{a}_n(\xi(r_t), \psi_t) = \mathbf{a}_n(\psi_t) \odot \mathbf{e}(\xi(r_t)) \quad (26a)$$

$$\begin{aligned} \mathbf{e}(\xi(r_t)) &= \\ [e_1(-\xi(r_t)), e_2(-\xi(r_t)), \dots, e_{N_T}(-\xi(r_t))]^T, \end{aligned} \quad (26b)$$

with \odot denoting the Hadamard matrix product,

$$\mathbf{\Omega}^{m'}(t_l, \varphi) = \text{diag}\{\omega^{m'}(t_l, \varphi)\} \quad (27a)$$

$$\begin{aligned} \omega^{m'}(t_l, \varphi) &= \mathbf{\Omega}(t_l, \varphi) \mathbf{e}^{m'}(t_l) \\ &= \omega_D(t_l, \varphi) \odot \mathbf{e}^{m'}(t_l) \end{aligned} \quad (27b)$$

$$\begin{aligned} \mathbf{e}^{m'}(t_l) &= \\ [e^{j2\pi(1-m')\Delta f t_l}, e^{j2\pi(2-m')\Delta f t_l}, \dots, e^{j2\pi(N_T-m')\Delta f t_l}]^T, \end{aligned} \quad (27c)$$

and

$$\begin{aligned} \mathbf{u}^{m'}(\tau; \xi(r_t); \mathbf{w}) &= \\ &= \mathbf{U}(\tau; \xi(r_t); \mathbf{w}) \mathbf{e}^{m'}(\tau) \\ &= \text{rect}\left(\frac{\tau - \xi(r_t)}{T_p}\right) u(\tau - \xi(r_t)) \mathbf{w} \odot \mathbf{e}^{m'}(\tau) \end{aligned} \quad (28a)$$

$$\begin{aligned} \mathbf{e}^{m'}(\tau) &= \\ [e^{j2\pi(1-m')\Delta f \tau}, e^{j2\pi(2-m')\Delta f \tau}, \dots, e^{j2\pi(N_T-m')\Delta f \tau}]^T \end{aligned} \quad (28b)$$

Here, the symbol $\hat{\tau}$ denotes the processing in the fast-time domain.

D. Matched Filtering

To obtain the pulse compression gain, one proceeds to form a matched filtering in the fast-time domain, with the filter

¹High-speed maneuvering targets will cause range migration (RM) and Doppler frequency migration (DFM) resulting in that a target will be more difficult to detect. We note that long-time coherent integration by compensating range walk and phase modulations over different sampling pulses is an effective method to improve radar target detection performance [23], [24]

output of the m' -th channel being the signal

$$\begin{aligned}\bar{r}_{m',n}(t_l, \hat{\tau}) &= r_{m',n}(t_l, \hat{\tau}) * h(\tau) \\ &= \delta_t \mathbf{a}_n^T(\xi(r_t), \psi_t) \mathbf{\Omega}^{m'}(t_l, \varphi) \mathbf{g}^{m'}(\tau; \mathbf{w})\end{aligned}\quad (29)$$

where

$$h(\tau) = u^c(\tau) \quad (30)$$

denotes the matched waveform, and

$$\mathbf{g}^{m'}(\tau; \mathbf{w}) = \left[g_1^{m'}(\tau; w_1), g_2^{m'}(\tau; w_2), \dots, g_{N_T}^{m'}(\tau; w_{N_T}) \right] \quad (31)$$

where

$$\begin{aligned}g_m^{m'}(\tau; w_m) &= w_m \left[u(\tau - \xi(r_t)) e^{j2\pi(m-m')\Delta f \tau} \right] * h(\tau) \\ &= w_m \int_{T_P} u(\beta - \xi(r_t)) e^{j2\pi(m-m')\Delta f \beta} u^c(\beta - \tau) d\beta \\ &= w_m e^{j2\pi(m-m')\Delta f \xi(r_t)} \\ &\quad \times \int_{T_P} u(\beta) e^{j2\pi(m-m')\Delta f \beta} u^c(\beta + \xi(r_t) - \tau) d\beta \\ &= w_m \mathbb{G}(\tau - \xi(r_t), (m - m')\Delta f)\end{aligned}\quad (32)$$

with

$$\mathbb{G}(\tau', f') = \int_{T_P} u(\tau) e^{j2\pi\tau f'} u^c(\tau - \tau') d\tau \quad (33)$$

being the ambiguity function of $u(\tau)$, implying that when $m = m'$, the maximum occurs at the target's round trip delay, i.e., $\tau = \xi(r_t)$.

E. Doppler Demodulation

The third step is Doppler demodulation in the slow-time domain, shifting the m' -th channel signal to the baseband in the Doppler domain. In order to do so, (29) is expressed as

$$\bar{r}_{m',n}(t_l, \hat{\tau}) = \delta_t \mathbf{a}_n^T(\xi(r_t), \psi_t) \mathbf{G}^{m'}(\tau; \mathbf{w}) \omega^{m'}(t_l, \varphi) \quad (34)$$

where

$$\mathbf{G}^{m'}(\tau; \mathbf{w}) = \text{diag} \left\{ \mathbf{g}^{m'}(\tau; \mathbf{w}) \right\} \quad (35a)$$

$$\omega^{m'}(t_l; \varphi) = \omega_{D,m'}(t_l, \varphi_{m'}) e^{j2\pi m' \Delta f t_l} \quad (35b)$$

with $\mathbf{a}_n(\xi(r_t), \psi_t)$ as given in (26a). Then, the Doppler demodulation may be performed by using the modulated slow-time signal $e^{-j2\pi\varphi_{m'} t_l}$, yielding the demodulated signal

$$\begin{aligned}\tilde{r}_{m',n}(\hat{t}_l, \tau) &= \sum_{m=1}^{N_T} \left\{ \bar{r}_{m',n}(\hat{t}_l, \tau) e^{-j2\pi\varphi_{m'} t_l} \right\} \\ &= \sum_{m=1}^{N_T} \left\{ \mu_{m,n}^{m'}(\tau; r_t, \psi_t) e^{j2\pi[D_m - D_{m'}]t_l} \right\} \\ &= \mu_{m',n}^{m'}(\tau; r_t, \psi_t) e^{j2\pi \frac{f_{m'}}{f_c} f_d t_l} \\ &\quad + \underbrace{\sum_{\substack{m=1 \\ m \neq m'}}^{N_T} \left\{ \mu_{m,n}^{m'}(\tau; r_t, \psi_t) e^{j2\pi[D_m - D_{m'}]t_l} \right\}}_{\text{aliased term}}\end{aligned}\quad (36)$$

where

$$\mu_{m,n}^{m'}(\tau; r_t, \psi_t) = \delta_t a_{m,n}(\xi(r_t), \psi_t) g_m^{m'}(\tau; w_m) \quad (37a)$$

$$D_m = \frac{f_c + (m-1)\Delta f}{f_c} f_{t,d} + m\Delta f + \varphi_m \quad (37b)$$

Here, the symbol \hat{t}_l denotes the processing in the slow-time domain.

F. Low-pass Filtering

Note that by designing the phase code φ_m , it is possible to make the Doppler of the aliased term and the Doppler of the desired signal $\mu_{m',n}^{m'}(\tau; r_t, \psi_t) e^{j2\pi \frac{f_{m'}}{f_c} f_d t_l}$ belong to different Doppler bands. Accordingly, under the condition that the target Doppler $f_{t,d}$ is smaller than $\frac{\text{PRF}}{N_T}$, where PRF denotes the pulse repetition frequency, the constraints that need to be imposed on the phase code φ_m are given in (38), shown at the top of the next page, where the N_T different Doppler frequencies, $\{D_m\}_{m=1}^{N_T}$, given in (37b), are forced to lie in the unambiguous Doppler domain with a mutual Doppler gap of $\frac{\text{PRF}}{N_T}$. As a result, applying a low-pass filter with cutoff frequency $\frac{\text{PRF}}{N_T}$ in the Doppler domain, the aliased term can be filtered out.

Thus, sampling the signal $\tilde{r}_{m',n}(\hat{t}_l, \tau)$ at $\tau = \xi(r_t)$ and then stacking the L outputs obtained by the low-pass filtering yields

$$\begin{aligned}\tilde{\mathbf{r}}_{m',n}(r_t) &= \tilde{\mathbf{r}}_{m',n}(t_l, r_t) * \bar{\mathbf{h}}(t_l) \\ &= \mu_{m',n}^{m'}(r_t) \mathbf{b}_{\text{dop}}^{m'}(f_{t,d})\end{aligned}\quad (39)$$

where

$$\begin{aligned}\tilde{\mathbf{r}}_{m',n}(t_l, r_t) &= [\tilde{r}_{m',n}(t_1, r_t), \tilde{r}_{m',n}(t_2, r_t), \dots, \tilde{r}_{m',n}(t_L, r_t)]^T\end{aligned}\quad (40a)$$

$$\tilde{r}_{m',n}(t_1, r_t) = \tilde{r}_{m',n}(t_1, \tau = \xi(r_t)), \quad (40b)$$

$$\begin{aligned}\mu_{m',n}^{m'}(r_t) &= \mu_{m',n}^{m'}(\tau = \xi(r_t); r_t, \psi_t) \\ &= \delta_t a_{m,n}(\xi(r_t), \psi_t) g_m^{m'}(\tau = \xi(r_t); w_m) \\ &= \delta_t a_{m,n}(\xi(r_t), \psi_t) w_m \mathbb{G}(0, 0),\end{aligned}\quad (41)$$

$$\mathbf{b}_{\text{dop}}^{m'}(f_{t,d}) = \begin{bmatrix} e^{j2\pi \frac{f_c + (m'-1)\Delta f}{f_c} f_{t,d} t_1} \\ e^{j2\pi \frac{f_c + (m'-1)\Delta f}{f_c} f_{t,d} t_2} \\ \dots \\ e^{j2\pi \frac{f_c + (m'-1)\Delta f}{f_c} f_{t,d} t_L} \end{bmatrix}, \quad (42)$$

with $\bar{\mathbf{h}}(t_l) \in \mathbb{C}^{L \times 1}$ denoting the low-pass filter function in the Doppler domain. With N_R receive antennas, each of which has N_T channels, the received data for one CPI comprises $N_T N_R L$ complex samples. Thus, the $N_T N_R L \times 1$ -dimensional space-time snapshot can be obtained as

$$\begin{aligned}\mathbf{q}_{\text{tar}}(r_t, \psi_t, f_{t,d}; \mathbf{w}) &= \delta_t \mathbb{G}(0, 0) \\ &\quad \times \text{vec} \left\{ \begin{bmatrix} \mathbf{k}_1(\mathbf{w}) & \mathbf{k}_2(\mathbf{w}) & \dots & \mathbf{k}_L(\mathbf{w}) \end{bmatrix} \right\}\end{aligned}\quad (43)$$

$$\left\{ \varphi_m \left| \begin{array}{l} D_{m+1} - D_m \geq \frac{\text{PRF}}{N_T} \\ D_{N_T} \leq \text{PRF} \end{array} \right. \right\} = \left\{ \varphi_m \left| \begin{array}{l} \frac{\Delta f}{f_c} f_{t,d} + \Delta f + \varphi_{m+1} - \varphi_m \geq \frac{\text{PRF}}{N_T} \\ \frac{f_{N_T}}{f_c} f_{t,d} + N_T \Delta f + \varphi_{N_T} \leq \text{PRF} \end{array} \right. \right\} \quad (38a)$$

$$\left\{ \varphi_m \left| \begin{array}{l} D_{m+1} - D_m \geq \frac{\text{PRF}}{N_T} \\ D_{N_T} \geq \text{PRF} \\ D_1 - (D_{N_T} - \text{PRF}) \geq \frac{\text{PRF}}{N_T} \end{array} \right. \right\} = \left\{ \varphi_m \left| \begin{array}{l} \frac{\Delta f}{f_c} f_{t,d} + \Delta f + \varphi_{m+1} - \varphi_m \geq \frac{\text{PRF}}{N_T} \\ \frac{f_{N_T}}{f_c} f_{t,d} + N_T \Delta f + \varphi_{N_T} \geq \text{PRF} \\ \frac{(1-N_T)\Delta f}{f_c} f_{t,d} + (1-N_T)\Delta f + \varphi_1 - \varphi_{m+1} + \text{PRF} \geq \frac{\text{PRF}}{N_T} \end{array} \right. \right\} \quad (38b)$$

where

$$\mathbf{k}_l(\mathbf{w}) = (\mathbf{I}_{N_R} \otimes \text{diag}\{\mathbf{w} \odot \bar{\mathbf{b}}_{dop,l}\}) \begin{bmatrix} \mathbf{a}_1(\xi(r_t), \psi_t) \\ \mathbf{a}_2(\xi(r_t), \psi_t) \\ \dots \\ \mathbf{a}_{N_R}(\xi(r_t), \psi_t) \end{bmatrix} \quad (44a)$$

$$\bar{\mathbf{b}}_{dop,l} = \begin{bmatrix} e^{j2\pi f_{t,d} t_l} \\ e^{j2\pi \frac{f_c + \Delta f}{f_c} f_{t,d} t_l} \\ \dots \\ e^{j2\pi \frac{f_c + (N_T - 1)\Delta f}{f_c} f_{t,d} t_l} \end{bmatrix} \quad (44b)$$

for $l = 1, 2, \dots, L$. Considering that $\Delta f \ll f_c$

$$\begin{aligned} a_{m,n}(\psi_t) &= e^{j2\pi(f_c + (m-1)\Delta f)[(m-1)\xi_T(\psi_t) + (n-1)\xi_R(\psi_t)]} \\ &\approx e^{j2\pi(f_c + (m-1)\Delta f)(m-1)\xi_T(\psi_t)} e^{j2\pi f_c(n-1)\xi_R(\psi_t)}, \end{aligned} \quad (45)$$

allowing (43) to be approximated as

$$\begin{aligned} \mathbf{q}_{tar}(r_t, \psi_t, f_{t,d}; \mathbf{w}) &\approx \delta_t \mathbb{G}(0, 0) \mathbf{b}_{dop}(f_{t,d}) \otimes (\mathbf{a}_R(\psi_t) \otimes [\mathbf{w} \odot \mathbf{a}_T(r_t, \psi_t)]) \\ &= \alpha_t \bar{\mathbf{q}}(r_t, \psi_t, f_{t,d}; \mathbf{w}) \end{aligned} \quad (46)$$

where \otimes denotes the Kronecker matrix product,

$$\alpha_t = \delta_t \mathbb{G}(0, 0) \quad (47a)$$

$$\mathbf{b}_{dop}(f_{t,d}) = [e^{j2\pi f_{t,d} t_1} \quad e^{j2\pi f_{t,d} t_2} \quad \dots \quad e^{j2\pi f_{t,d} t_L}]^T \quad (47b)$$

and

$$\bar{\mathbf{q}}(r, \psi, f_d; \mathbf{w}) = \mathbf{b}_{dop}(f_d) \otimes (\mathbf{a}_R(\psi) \otimes [\mathbf{w} \odot \mathbf{a}_T(r, \psi)]) \quad (48)$$

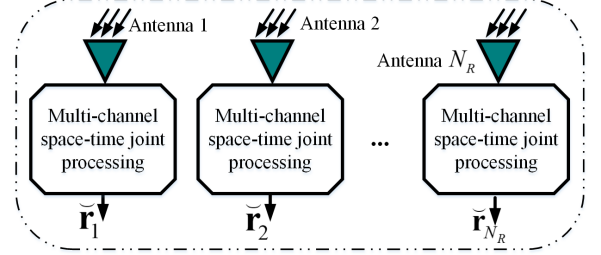
where

$$\mathbf{a}_T(r_t, \psi_t) = \mathbf{a}_T(\psi_t) \odot \mathbf{e}(\xi(r_t)) \quad (49a)$$

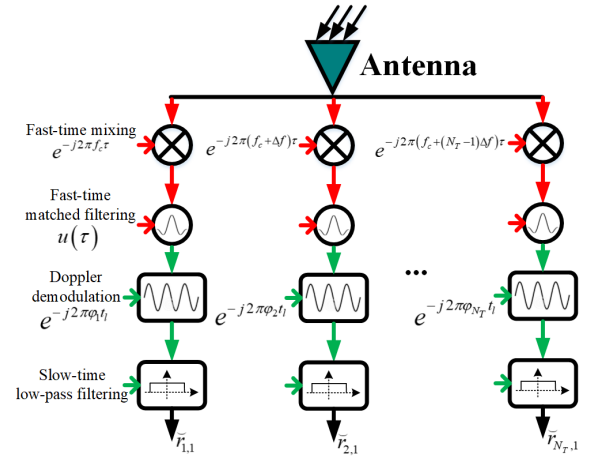
$$\mathbf{a}_T(\psi_t) = \begin{bmatrix} 1 \\ e^{j2\pi(f_c + \Delta f)\xi_T(\psi_t)} \\ \dots \\ e^{j2\pi(f_c + (N_T - 1)\Delta f)(N_T - 1)\xi_T(\psi_t)} \end{bmatrix} \quad (49b)$$

$$\mathbf{a}_R(\psi_t) = \begin{bmatrix} 1 \\ e^{j2\pi f_c \xi_R(\psi_t)} \\ \dots \\ e^{j2\pi f_c (N_R - 1)\xi_R(\psi_t)} \end{bmatrix} \quad (49c)$$

Fig. 3 shows the resulting proposed receiver for a coherent airborne FDA. For each receive antenna, a joint space-time processing module is applied to extract the desired signals from the aliased returns.



(a) The receiver structure.



(b) The joint space-time processing module.

Fig. 3. The proposed FDA receiver based on joint space-time processing.

IV. FDA RANGE-SPACE-TIME PROCESSING

A. Clutter Signal Model

For an airborne surveillance radar, the Earth's surface is the major source of clutter, which further complicates processing by the fact that the return from a discrete ground clutter source has the same form as a target echo. Since the ground is assumed to have zero inherent velocity, the relative Doppler of a ground clutter source depends only on its aspect with respect to the radar and on the platform velocity. Therefore, the clutter signal from the j -th clutter patch of range cell $r_{c,i}$ can be expressed as

$$\mathbf{q}_{clu,i,j}(\mathbf{w}) = \alpha_{c,i,j} \bar{\mathbf{q}}(r_{c,i}, \psi_{c,j}, f_{c,d,j}; \mathbf{w}), \quad (50)$$

for $j = 1, 2, \dots, J$, with J denoting the number of range cells, and $i = 1, 2, \dots, I$, with I denoting the number of clutter patches in an iso-range ring, where

$$f_{d,c,j} = \frac{2v_a}{\lambda} \cos \psi_{c,j} \quad (51)$$

and where $\alpha_{c,i,j}$ denotes the complex-valued clutter amplitude.

B. Jamming Signal Model

In this work, we only consider barrage jamming that is spatially correlated from element to element and temporally uncorrelated from pulse to pulse. Thus, the barrage jamming will temporally appear as thermal noise, but as a point target or a discrete clutter source in the spatial domain. The space-time snapshot of \tilde{j} -th jamming may be written as

$$\mathbf{q}_{jam,\tilde{j}} = \alpha_{jam,\tilde{j}} \bar{\mathbf{u}} \otimes \mathbf{a}_R(\psi_{jam,\tilde{j}}) \otimes \bar{\mathbf{u}} \quad (52)$$

for $\tilde{j} = 1, 2, \dots, \tilde{J}$, with \tilde{J} denoting the number of barrage jammers, where $\bar{\mathbf{u}} \in \mathbb{C}^{L \times 1}$ and $\bar{\mathbf{u}} \in \mathbb{C}^{N_T \times 1}$ are Gaussian random vectors.

C. Range-space-time Processing

Taking into account the clutter, jamming, and receiver noise, the coherent FDA receive data model may be expressed as

$$\begin{aligned} \mathbf{q} &= \mathbf{q}_{tar}(r_t, \psi_t, f_{t,d}; \mathbf{w}) \\ &+ \sum_i^I \sum_j^J \mathbf{q}_{clu,i,j}(\mathbf{w}) + \sum_{\tilde{j}}^{\tilde{J}} \mathbf{q}_{jam,\tilde{j}} + \mathbf{n} \\ &= \alpha_t \bar{\mathbf{q}}(r_t, \psi_t, f_{t,d}; \mathbf{w}) + \sum_i^I \sum_j^J \alpha_{c,i,j} \bar{\mathbf{q}}(r_{c,i}, \psi_{c,j}, f_{c,d,j}; \mathbf{w}) \\ &+ \sum_{\tilde{j}}^{\tilde{J}} \alpha_{jam,\tilde{j}} \bar{\mathbf{u}} \otimes \mathbf{a}_R(\psi_{jam,\tilde{j}}) \otimes \bar{\mathbf{u}} + \mathbf{n}. \end{aligned} \quad (53)$$

where $\mathbf{n} \in \mathbb{C}^{N_T N_R L \times 1}$ denotes an additive circularly symmetric Gaussian noise with power $|\alpha_{noise}|^2$. Employing a receiving beamformer $\mathbf{v} \in \mathbb{C}^{N_T N_R L \times 1}$ to synthesis the multiple channel outputs yields the output signal-to-interference-plus-noise ratio (SINR)

$$\begin{aligned} \psi(\mathbf{v}, \mathbf{w}) &= \frac{\mathbb{E} \left\{ |\mathbf{v}^H \mathbf{q}_{tar}(r_t, \psi_t, f_{t,d}; \mathbf{w})|^2 \right\}}{\mathbb{E} \left\{ |\mathbf{v}^H (\mathbf{q} - \mathbf{q}_{tar}(r_t, \psi_t, f_{t,d}; \mathbf{w}))|^2 \right\}} \\ &= \frac{\left| \mathbb{E} \left\{ \alpha_t \right\} \right|^2 \mathbf{v}^H \bar{\mathbf{q}}(r_t, \psi_t, f_{t,d}; \mathbf{w}) \bar{\mathbf{q}}^H(r_t, \psi_t, f_{t,d}; \mathbf{w}) \mathbf{v}}{\mathbf{v}^H \mathbf{R}_{cjn}(\mathbf{w}) \mathbf{v}} \\ &= \text{SNR} \cdot \frac{\mathbf{v}^H \bar{\mathbf{q}}(r_t, \psi_t, f_{t,d}; \mathbf{w}) \bar{\mathbf{q}}^H(r_t, \psi_t, f_{t,d}; \mathbf{w}) \mathbf{v}}{\mathbf{v}^H \mathbf{R}_{cjn}(\mathbf{w}) \mathbf{v}} \end{aligned} \quad (54)$$

where $\mathbb{E} \{ \cdot \}$ is the expectation operator and \mathbf{R}_{cjn} denotes the interference-plus-noise covariance matrix, given by

$$\begin{aligned} \mathbf{R}_{cjn}(\mathbf{w}) &= \mathbf{R}_{clu}(\mathbf{w}) + \mathbf{R}_{jam} + \mathbf{R}_{noise} \\ &= |\alpha_{noise}|^2 \bar{\mathbf{R}}_{cjn}(\mathbf{w}) \end{aligned} \quad (55)$$

where

$$\begin{aligned} \mathbf{R}_{clu}(\mathbf{w}) &= \mathbb{E} \left\{ \left(\sum_i^I \sum_j^J \mathbf{q}_{clu,i,j}(\mathbf{w}) \right) \left(\sum_i^I \sum_j^J \mathbf{q}_{clu,i,j}(\mathbf{w}) \right)^H \right\} \\ &= \mathbb{E} \left\{ |\alpha_{c,i,j}|^2 \right\} \\ &\quad \times \sum_i^I \sum_j^J \bar{\mathbf{q}}(r_{c,i}, \psi_{c,j}, f_{c,d,j}; \mathbf{w}) \bar{\mathbf{q}}^H(r_{c,i}, \psi_{c,j}, f_{c,d,j}; \mathbf{w}) \end{aligned} \quad (56)$$

denotes the clutter covariance matrix. Furthermore,

$$\begin{aligned} \mathbf{R}_{jam} &= \mathbb{E} \left\{ \left(\sum_{\tilde{j}}^{\tilde{J}} \mathbf{q}_{jam,\tilde{j}} \right) \left(\sum_{\tilde{j}}^{\tilde{J}} \mathbf{q}_{jam,\tilde{j}} \right)^H \right\} \\ &= \mathbf{I}_L \otimes \left[\sum_{\tilde{j}}^{\tilde{J}} \mathbb{E} \left\{ |\alpha_{jam,\tilde{j}}|^2 \right\} \mathbf{a}_R(\theta_{\tilde{j}}) \mathbf{a}_R^H(\theta_{\tilde{j}}) \right] \otimes \mathbf{I}_{N_T} \end{aligned} \quad (57)$$

denotes the jammer covariance matrix, with \mathbf{I}_K being the $K \times K$ -dimensional identity matrix,

$$\mathbf{R}_{noise} = \mathbb{E} \{ \mathbf{n} \mathbf{n}^H \} = |\alpha_{noise}|^2 \mathbf{I}_{N_T N_R L} \quad (58)$$

denotes the noise covariance matrix, and

$$\begin{aligned} \bar{\mathbf{R}}_{cjn}(\mathbf{w}) &= \sum_i^I \sum_j^J \text{CNR}_{i,j} \bar{\mathbf{q}}(r_{c,i}, \psi_{c,j}, f_{c,d,j}; \mathbf{w}) \bar{\mathbf{q}}^H(r_{c,i}, \psi_{c,j}, f_{c,d,j}; \mathbf{w}) \\ &+ \mathbf{I}_L \otimes \left[\sum_{\tilde{j}}^{\tilde{J}} \text{JNR}_{\tilde{j}} \mathbf{a}_R(\theta_{\tilde{j}}) \mathbf{a}_R^H(\theta_{\tilde{j}}) \right] \otimes \mathbf{I}_{N_T} + \mathbf{I}_{N_T N_R L} \end{aligned} \quad (59)$$

denotes the interference plus noise covariance matrix. Here, $\text{SNR} = \frac{\mathbb{E} \{ |\alpha_t|^2 \}}{|\alpha_{noise}|^2}$, $\text{CNR}_{i,j} = \frac{\mathbb{E} \{ |\alpha_{c,i,j}|^2 \}}{|\alpha_{noise}|^2}$, and $\text{JNR}_{\tilde{j}} = \frac{\mathbb{E} \{ |\alpha_{jam,\tilde{j}}|^2 \}}{|\alpha_{noise}|^2}$ denote the signal-to-noise ratio (SNR), the clutter-to-noise ratio (CNR), and the jamming-to-noise ratio (JNR), respectively. Consequently, the output SINR maximization problem can be formulated as

$$\max_{\mathbf{v}, \mathbf{w}} \frac{\mathbf{v}^H \bar{\mathbf{q}}(r_t, \psi_t, f_{t,d}; \mathbf{w}) \bar{\mathbf{q}}^H(r_t, \psi_t, f_{t,d}; \mathbf{w}) \mathbf{v}}{\mathbf{v}^H \bar{\mathbf{R}}_{cjn}(\mathbf{w}) \mathbf{v}}. \quad (60)$$

In practical applications, the optimization variables are often subject to many constraints. For example, constant modulus waveforms are often required due to the limitations of nonlinear radar amplifiers [25], [26]. Therefore, the above problem will typically also include multiple nonconvex constraints, making it a NP-hard problem which may not be solved efficiently [27]. However, it may be noted that the SINR can also be expressed as an explicit expression of the transmit weight vector, \mathbf{w} , as shown in the Appendix. This implies that an iterative optimization method based on a semidefinite relaxation (SDR) technique can be applied to solve it² [29]. In this

²How to solve the resulting non-convex problem more efficiently is beyond the scope of this paper, and interested readers are referred to [28] for a further discussion on these aspects.

TABLE I
SYSTEM PARAMETERS.

Parameter	Value	Parameter	Value
Number of transmit antennas	$N_T = 5$	Spacing of transmit array	$d_t = 0.125 \text{ m}$
Number of receive antennas	$N_R = 5$	Spacing of receive array	$d_r = 0.125 \text{ m}$
Pulse duration	$T_p = 1 \mu\text{s}$	Bandwidth of basedband LFM signal	20 MHz
Central carrier frequency	$f_c = 1.2 \text{ GHz}$	Frequency offset	$\Delta f = 1 \text{ MHz}$
Pulse repetition frequency	$\text{PRF} = 7 \text{ kHz}$	Wavelength	$\lambda = 0.25 \text{ m}$
Number of pulses	$L = 180$	Platform velocity	$v_a = 100 \text{ m/s}$

TABLE II
PARAMETER SETTINGS FOR SIMULATION SCENARIO.

Type	Target	Barrage jamming	Clutter
Range [km]	3.0	3.0	3.006
Azimuth angle	45°	120°	$(0, 180^\circ)$
Depression angle	45°	45°	45°
Doppler [Hz]	400	All Doppler	$(-565, 565)$
SNR/JNR/CNR [dB]	0	20	20

work, we consider uniform transmit weights, i.e., $\mathbf{w} = \mathbf{1}_{N_T \times 1}$, with $\mathbf{1}_{N_T \times 1}$ denoting the $N_T \times 1$ -dimensional all-ones vector, converting (60) to a minimum variance distortionless response (MVDR) problem, whose solution is given by (see, e.g., [25], [28])

$$\mathbf{v} = \frac{\bar{\mathbf{R}}_{cjn}^{-1}(\mathbf{w} = \mathbf{1}_{N_T \times 1}) \bar{\mathbf{q}}_{\text{target}, \mathbf{w} = \mathbf{1}_{N_T \times 1}}}{\bar{\mathbf{q}}_{\text{target}, \mathbf{w} = \mathbf{1}_{N_T \times 1}}^H \bar{\mathbf{R}}_{cjn}^{-1}(\mathbf{w} = \mathbf{1}_{N_T \times 1}) \bar{\mathbf{q}}_{\text{target}, \mathbf{w} = \mathbf{1}_{N_T \times 1}}} \quad (61)$$

where $\bar{\mathbf{q}}_{\text{target}, \mathbf{w} = \mathbf{1}_{N_T \times 1}} = \bar{\mathbf{q}}(r_t, \psi_t, f_t, d; \mathbf{w} = \mathbf{1}_{N_T \times 1})$. As the covariance matrix $\bar{\mathbf{R}}_{cjn}(\mathbf{w})$ for an FDA radar is range-dependent, it has to be estimated according to the actual scattering scenario, instead of using secondary data obtained from nearby range cells as is done in conventional radars [30]. As the estimation procedure is not the focus of this paper, the following simulations assume full knowledge of the covariance matrix. It is worth noting that since the transmit weights provide more degrees of freedom to increase the SINR, the joint design in (60) can be expected to obtain a higher SINR.

V. SIMULATION

In this section, numerical simulations are provided to evaluate the effectiveness of the proposed receiver and the performance of the joint range-space-time processing. Herein, we only consider clutter that is within the same range cell as the target. Unless otherwise specified, in all simulations, the FDA system parameters are as listed in Tab. I. Noting the relationship between the clutter Doppler and the platform velocity, given in (51), the range of values for the clutter Doppler is $(-565, 565) \text{ Hz}$. The parameters for the simulation scenarios are listed in Tab. II.

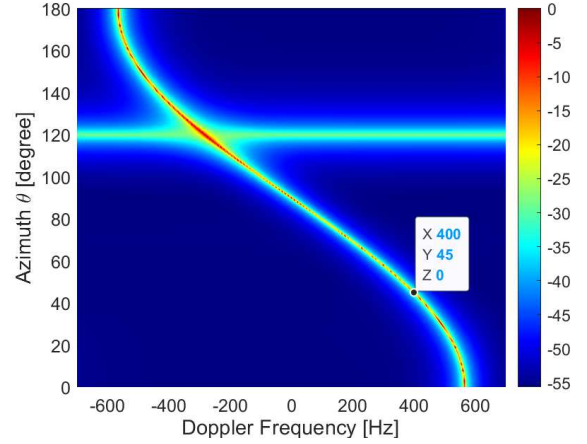


Fig. 4. The energy distribution of the interferences in the Doppler-azimuth domain. The marked position is that of the target, which can be seen to be entirely obscured by the clutter ridge.

A. Adapted Patterns

Fig. 4 shows the energy of the interferences distributed in the Doppler-azimuth domain, $P(f_d, \psi)$, as calculated by

$$P(\psi, f_d) = \frac{1}{\bar{\mathbf{q}}^H(r_t, \psi, f_d) \bar{\mathbf{R}}_{cjn}^{-1}(\mathbf{w}) \bar{\mathbf{q}}(r_t, \psi, f_d; \mathbf{w})} \Big|_{\mathbf{w} = \mathbf{1}_{N_T \times 1}}. \quad (62)$$

We refer the reader to (11) for the conversion of the conic angle and the azimuth angle. As may be seen, the target is fully obscured by the clutter ridge. The adapted pattern, as a function of angle and Doppler, is an important performance metric, defined by

$$\bar{P}(\psi, f_d) = |\mathbf{v}^H \bar{\mathbf{q}}(r_t, \psi, f_d; \mathbf{w} = \mathbf{1}_{N_T \times 1})|^2. \quad (63)$$

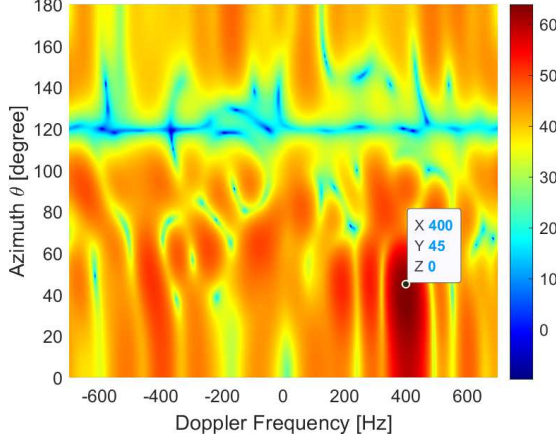


Fig. 5. The output power distribution after implementing the joint range-space-time processing. The marked position is that of the target.

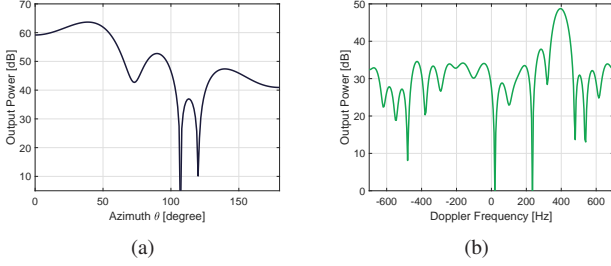


Fig. 6. Cuts of the FDA adapted pattern (a) at the Doppler frequency $f_d = 400$ Hz, and (b) at the azimuth angle $\theta = 45^\circ$.

where for each angle-Doppler pair (ψ, f_d) , the receive weight vector \mathbf{v} is computed using (61). Ideally, the pattern has nulls in the locations of interference sources and high gain at the angle and Doppler of the presumed target direction. Fig. 5 shows the adapted pattern behavior, with Figs. 6a and 6b showing the cuts of this pattern at the azimuth angle $\theta = 45^\circ$ and the Doppler frequency $f_d = 400$ Hz, respectively. One may note that the resulting pattern can form a mainlobe at the target location, with deep nulls at the locations of the jammer and clutter sources. In comparison, the results of the MIMO and the phased-array systems are shown in Figs. 7a and 7b, respectively, with the corresponding cuts shown in Fig. 8. It is worth noting that for the MIMO and the phased-array systems, deep nulls appear along both the jamming and clutter lines. However, there is no peak at the target location due to the lack of range-controllable degrees of freedom.

B. SINR Loss

It is often useful to express the performance relative to what could be obtained in the absence of interferences. The SINR loss, $L_{SINR}(\psi, f_d)$, is defined to be the processed performance relative to what could be obtained in an interference-free environment, i.e.,

$$L_{SINR}(\psi, f_d) = 20 \log_{10} \left(\frac{|\mathbf{v}^H \bar{\mathbf{q}}(r_t, \psi, f_d; \mathbf{w} = \mathbf{1}_{N_T \times 1})|}{N_T N_R L} \right). \quad (64)$$

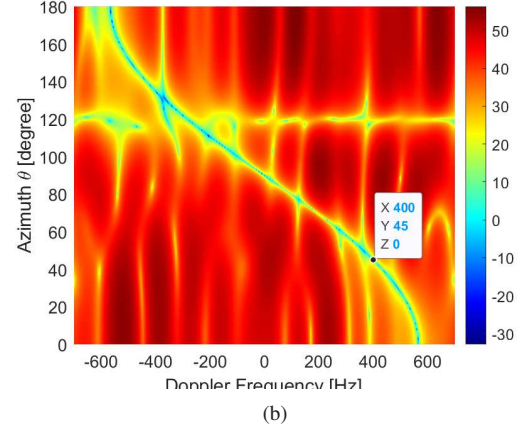
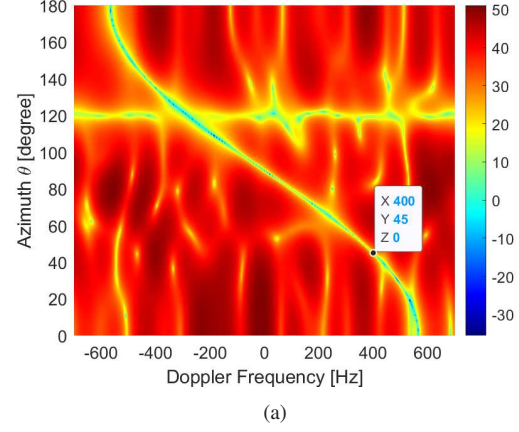


Fig. 7. The output power distribution of (a) a MIMO and (b) a phased-array system. The marked position is that of the target.

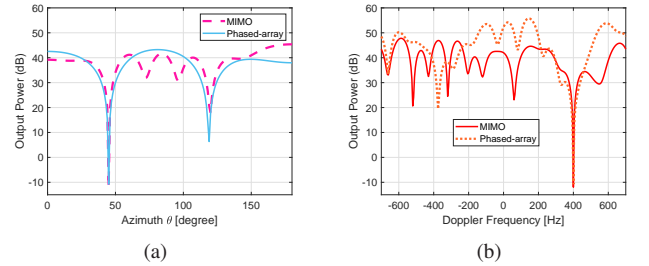


Fig. 8. The cuts of the MIMO and the phased-array adapted patterns (a) at the Doppler frequency $f_d = 400$ Hz, and (b) at the azimuth angle $\theta = 45^\circ$.

The gain of $N_T N_R L$ represents the coherent spatial and temporal integration over the virtual $N_T N_R$ elements and the L pulses. It may be noted that L_{SINR} is a function of Doppler and azimuth. However, it is usually plotted as a function of Doppler, assuming that the array is oriented in the desired target direction. Fig. 9 shows the SINR loss curves obtained by the FDA, MIMO, and phased-array systems, where the azimuth angle is fixed at $\theta = 90^\circ$. As expected, when the target velocity is close to zero Doppler, the performance loss of the FDA is very small as compared to the MIMO and the phased-array systems.

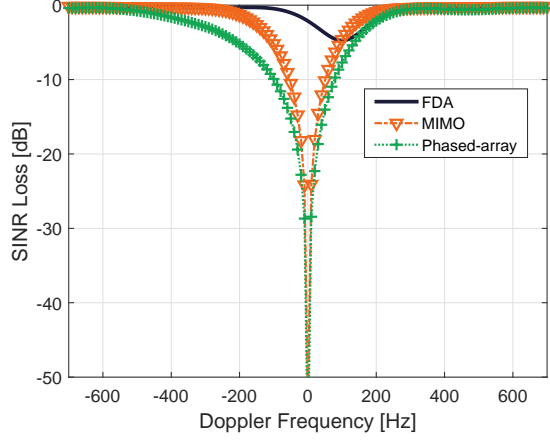


Fig. 9. The SINR loss curves obtained by FDA, MIMO and phased-array systems.

VI. CONCLUSION

In this paper, using range-controllable degrees of freedom, we present a method for high-gain detection of an airborne FDA radar for targets obscured by mainlobe clutter with the same Doppler frequency. In order to do so, a receiver for coherent FDA is proposed that takes full advantage of the orthogonality of the echo signals in the Doppler domain. For each receive antenna, a joint space-time processing module is applied to extract the desired signals from the aliased returns. Then, the receive signal model considering the ground clutter and the barrage jamming is devised. Finally, the target detection is formed using an adapted MVDR spatial-temporal receiver. The proposed joint range-space-time processing method is also easily extendable with additional constraints that may occur in practice, although even so, the output SINR can be expected to improve by jointly designing the transmit and receive weights.

APPENDIX

Using the equality

$$\mathbf{p}_{M \times 1} \otimes \mathbf{b}_{N \times 1} = \left((\mathbf{b}_{N \times 1})^H \left[(\mathbf{p}_{M \times 1})^H \otimes \mathbf{I}_N \right] \right)^H \quad (65)$$

$$= (\mathbf{p}_{M \times 1} \otimes \mathbf{I}_N) \mathbf{b}_{N \times 1}$$

where $\mathbf{p}_{M \times 1}$ and $\mathbf{b}_{N \times 1}$ denote the $M \times 1$ - and $N \times 1$ -dimensional vectors, respectively, the vector $\bar{\mathbf{q}}(r, \psi, f_d; \mathbf{w})$ can be equivalently expressed as

$$\begin{aligned} \bar{\mathbf{q}}(r, \psi, f_d; \mathbf{w}) &= \mathbf{b}_{\text{dop}}(f_d) \otimes (\mathbf{a}_R(\psi) \otimes [\mathbf{w} \odot \mathbf{a}_T(r, \psi)]) \\ &= (\mathbf{b}_{\text{dop}}(f_d) \otimes \mathbf{I}_{N_T N_R}) (\mathbf{a}_R(\psi) \otimes [\mathbf{w} \odot \mathbf{a}_T(r, \psi)]) \\ &= (\mathbf{b}_{\text{dop}}(f_d) \otimes \mathbf{I}_{N_T N_R}) (\mathbf{a}_R(\psi) \otimes \mathbf{I}_{N_T}) [\mathbf{w} \odot \mathbf{a}_T(r, \psi)] \\ &= \mathbf{C}(r, \psi, f_d) \mathbf{w} \end{aligned} \quad (66)$$

where

$$\begin{aligned} \mathbf{C}(r, \psi, f_d) &= (\mathbf{b}_{\text{dop}}(f_d) \otimes \mathbf{I}_{N_T N_R}) \\ &\quad \times (\mathbf{a}_R(\psi) \otimes \mathbf{I}_{N_T}) \text{diag}\{\mathbf{a}_T(r, \psi)\}. \end{aligned} \quad (67)$$

Substituting (66) into (54) yields

$$\psi(\mathbf{v}, \mathbf{w}) = \text{SNR} \cdot \frac{\mathbf{w}^H \mathbf{C}_t(\mathbf{v}) \mathbf{w}}{\mathbf{w}^H \mathbf{C}_c(\mathbf{v}) \mathbf{w} + \eta(\mathbf{v})} \quad (68)$$

where

$$\mathbf{C}_t(\mathbf{v}) = \mathbf{C}^H(r_t, \psi_t, f_{t,d}) \mathbf{v} \mathbf{v}^H \mathbf{C}(r_t, \psi_t, f_{t,d}) \quad (69a)$$

$$\mathbf{C}_c(\mathbf{v}) =$$

$$\sum_i \sum_j \text{CNR}_{i,j} \mathbf{C}^H(r_{c,j}, \psi_{c,j}, f_{c,d,j}) \mathbf{v} \mathbf{v}^H \mathbf{C}(r_{c,j}, \psi_{c,j}, f_{c,d,j}) \quad (69b)$$

$$\begin{aligned} \eta(\mathbf{v}) &= \mathbf{v}^H \left(\mathbf{I}_L \otimes \left[\sum_{\tilde{j}} \text{JNR}_{\tilde{j}} \mathbf{a}_R(\theta_{\tilde{j}}) \mathbf{a}_R^H(\theta_{\tilde{j}}) \right] \otimes \mathbf{I}_{N_T} \right) \mathbf{v} \\ &\quad + \mathbf{v}^H \mathbf{I}_{N_T N_R L} \mathbf{v} \end{aligned} \quad (69c)$$

which completes the proof.

REFERENCES

- [1] M. I. Skolnik, "Introduction to radar systems," *New York*, 1980.
- [2] R. Klemm, *Principles of space-time adaptive processing*. IET, 2002, no. 12.
- [3] P. Antonik, M. Wicks, H. Griffiths, and C. Baker, "Frequency diverse array radars," in *2006 IEEE Conference on Radar*, Verona, NY, USA, 2006, pp. 215–217.
- [4] P. Antonik, M. C. Wicks, H. D. Griffiths, and C. J. Baker, "Range-dependent beamforming using element level waveform diversity," in *2006 International Waveform Diversity Design Conference*, Lihue, HI, USA, 2006, pp. 1–6.
- [5] L. Lan, J. Xu, G. Liao, Y. Zhang, F. Fioranelli, and H. C. So, "Suppression of mainbeam deceptive jammer with FDA-MIMO radar," *IEEE Transactions on Vehicular Technology*, vol. 69, no. 10, pp. 11 584–11 598, 2020.
- [6] R. Gui, W.-Q. Wang, A. Farina, and H. C. So, "FDA radar with doppler-spreading consideration: Mainlobe clutter suppression for blind-doppler target detection," *Signal Processing*, vol. 179, p. 107773, 2021.
- [7] W.-Q. Wang and H. C. So, "Transmit subaperturing for range and angle estimation in frequency diverse array radar," *IEEE Transactions on Signal Processing*, vol. 62, no. 8, pp. 2000–2011, 2014.
- [8] J. Xu, G. Liao, S. Zhu, L. Huang, and H. C. So, "Joint range and angle estimation using MIMO radar with frequency diverse array," *IEEE Transactions on Signal Processing*, vol. 63, no. 13, pp. 3396–3410, 2015.
- [9] J. Xiong, W.-Q. Wang, and K. Gao, "FDA-MIMO radar range-angle estimation: CRLB, MSE, and resolution analysis," *IEEE Transactions on Aerospace and Electronic Systems*, vol. 54, no. 1, pp. 284–294, 2018.
- [10] W.-Q. Wang, "Moving-target tracking by cognitive RF stealth radar using frequency diverse array antenna," *IEEE Transactions on Geoscience and Remote Sensing*, vol. 54, no. 7, pp. 3764–3773, 2016.
- [11] R. Gui, Z. Zheng, and W.-Q. Wang, "Cognitive FDA radar transmit power allocation for target tracking in spectrally dense scenario," *Signal Processing*, vol. 183, p. 108006, 2021.
- [12] W.-Q. Wang, "Range-angle dependent transmit beampattern synthesis for linear frequency diverse arrays," *IEEE Transactions on Antennas and Propagation*, vol. 61, no. 8, pp. 4073–4081, 2013.
- [13] J. Xiong, W.-Q. Wang, H. Shao, and H. Chen, "Frequency diverse array transmit beampattern optimization with genetic algorithm," *IEEE Antennas and Wireless Propagation Letters*, vol. 16, pp. 469–472, 2016.
- [14] H. Chen, H.-Z. Shao, and W.-Q. Wang, "Joint sparsity-based range-angle-dependent beampattern synthesis for frequency diverse array," *IEEE Access*, vol. 5, pp. 15 152–15 161, 2017.
- [15] H. Wang, G. Liao, J. Xu, and S. Zhu, "Transmit beampattern design for coherent FDA by piecewise LFM waveform," *Signal Processing*, vol. 161, pp. 14–24, 2019.
- [16] J. Xu, J. Kang, G. Liao, and H. C. So, "Mainlobe deceptive jammer suppression with FDA-MIMO radar," in *2018 IEEE 10th Sensor Array and Multichannel Signal Processing Workshop (SAM)*, 2018, pp. 504–508.

- [17] L. Lan, G. Liao, J. Xu, Y. Zhang, and B. Liao, "Transceive beamforming with accurate nulling in FDA-MIMO radar for imaging," *IEEE Transactions on Geoscience and Remote Sensing*, vol. 58, no. 6, pp. 4145–4159, 2020.
- [18] L. Lan, M. Rosamilia, A. Aubry, A. De Maio, and G. Liao, "Single-snapshot angle and incremental range estimation for FDA-MIMO radar," *IEEE Transactions on Aerospace and Electronic Systems*, vol. 57, no. 6, pp. 3705–3718, 2021.
- [19] R. Gui, W.-Q. Wang, C. Cui, and H. C. So, "Coherent pulsed-FDA radar receiver design with time-variance consideration: Sinr and crb analysis," *IEEE Transactions on Signal Processing*, vol. 66, no. 1, pp. 200–214, 2018.
- [20] H. Wang, Y. Quan, G. Liao, S. Zhu, J. Xu, and L. Huang, "Space-time coding technique for coherent frequency diverse array," *IEEE Transactions on Signal Processing*, vol. 69, pp. 5994–6008, 2021.
- [21] R. Gui and W.-Q. Wang, "Adaptive transmit power allocation for FDA radar with spectral interference avoidance," in *2020 IEEE Radar Conference (RadarConf20)*, Florence, Italy, 2020, pp. 1–6.
- [22] M. A. Richards, *Fundamentals of radar signal processing*. McGraw-Hill Education, 2014.
- [23] J. Xu, J. Yu, Y.-N. Peng, and X.-G. Xia, "Radon-fourier transform for radar target detection, i: generalized doppler filter bank," *IEEE transactions on aerospace and electronic systems*, vol. 47, no. 2, pp. 1186–1202, 2011.
- [24] W. Jia, Y. Cao, S. Zhang, and W.-Q. Wang, "Detecting high-speed maneuvering targets by exploiting range-Doppler relationship for lfm radar," *IEEE Transactions on Vehicular Technology*, vol. 70, no. 3, pp. 2209–2218, 2021.
- [25] G. Cui, H. Li, and M. Rangaswamy, "MIMO radar waveform design with constant modulus and similarity constraints," *IEEE Transactions on Signal Processing*, vol. 62, no. 2, pp. 343–353, 2014.
- [26] O. Aldayel, V. Monga, and M. Rangaswamy, "Successive QCQP refinement for MIMO radar waveform design under practical constraints," *IEEE Transactions on Signal Processing*, vol. 64, no. 14, pp. 3760–3774, 2016.
- [27] S. Boyd, S. P. Boyd, and L. Vandenberghe, *Convex optimization*. Cambridge university press, 2004.
- [28] Z. Cheng, B. Liao, Z. He, J. Li, and J. Xie, "Joint design of the transmit and receive beamforming in MIMO radar systems," *IEEE Transactions on Vehicular Technology*, vol. 68, no. 8, pp. 7919–7930, 2019.
- [29] Z.-q. Luo, W.-k. Ma, A. M.-c. So, Y. Ye, and S. Zhang, "Semidefinite relaxation of quadratic optimization problems," *IEEE Signal Processing Magazine*, vol. 27, no. 3, pp. 20–34, 2010.
- [30] L. Wang, W.-Q. Wang, and H. C. So, "Covariance matrix estimation for FDA-MIMO adaptive transmit power allocation," *IEEE Transactions on Signal Processing*, 2022.